FULL PAPER

ADVANCED FUNCTIONAL MATERIALS

DOI: 10.1002/adfm.200600790

Forming Antifouling Organic Multilayers on Porous Silicon Rugate Filters Towards In Vivo/Ex Vivo Biophotonic Devices**

By *Kristopher A. Kilian*, *Till Böcking*, *Suhrawardi Ilyas*, *Katharina Gaus*, *Wendy Jessup*, *Michael Gal*,* and *J. Justin Gooding**

We describe the development and optimization of porous silicon photonic crystal surface chemistry towards implantable optical devices. Porous silicon rugate filters were prepared to obtain a narrow linewidth reflectivity peak in the near-infrared (700–1000 nm) with low background reflectivity elsewhere. The morphology of the mesoporous structures (pore diameter < 50 nm) was such that only small proteins could infiltrate the pores whereas larger proteins were excluded. To provide stability in biological media, we established an approach to build organic multilayers containing hexa(ethylene oxide) moieties in porous silicon. The optical changes associated with organic derivatization were monitored concurrently with FTIR characterization. Furthermore, the antifouling capability of our chemical strategy is assessed and the penetration of different sized proteins into the structure was determined. The structural stability in biological environments was evaluated by incubation in human blood plasma over time while monitoring the optical signature of the photonic crystal.

1. Introduction

Advances in medical diagnostics towards in vivo and ex vivo devices relies heavily on development of transducers that are minimally invasive, highly sensitive and selective to analytes of interest and stable to biological enviroments. Minimally invasive optical devices have been developed for use intravascularly, extravascularly and subcutaneously with medical applications for monitoring during surgery, at the bedside and in point of care diagnosis.[1–4] One drawback to many optical systems is the need for molecular species at the biointerface that require excitation, often limiting the choice of analyte or requiring introduction of labelling compounds to the system. Furthermore, sophisticated microscopy instrumentation is required and the emitted light oftentimes interacts adversely with tissue,[5] confounding accurate detection and read-out. Minimally invasive fibreoptic devices using external light sources and lasers to interrogate the refractive index change at the biorecognition interface have shown promise, obviating the need for labelling schemes.[6,7] Although methods using evanescent fields such as surface plasmon resonance or resonant mirror techniques eliminate the need for labels, external contact with the device remains a requirement. Non-invasive read-out of implantable photonic structures is an interesting alternative to these methods, made possible by engineering devices which respond within the optical window of tissue (near-IR, 700–1000 nm). Using the intrinsic properties of photonic materials, detection relies on a change in the wavelength of reflected light induced by refractive index changes upon biorecognition. This approach allows more control over optical path lengths, avoiding light scattering effects common to fiberoptic transduction whilst enabling a simple method for real time monitoring. Detection of molecular species in a patients blood stream (in vivo, ex vivo) or subcutaneous environement can then be performed merely by irradiating the area with a light source whilst collecting the reflected spectrum.

One material that has enormous potential for implantable photonic devices is porous silicon.[8] The interest in porous silicon is due to the ease and quality of manufacturing, a large internal surface area for analyte binding, an inherant biocompatability and the ability to tune the optical properties of porous silicon photonic crystals with unprecedented control.[9] Porous silicon is formed by anodic etching of silicon in ethanolic hydrofluoric acid solution. The porosity of the material is directly proportional to the applied current density during the electrochemical etch, thus allowing control over the average refractive index of the material. Porous silicon based rugate filters are a class of multilayered photonic crystal with a sinusoidal refractive index distribution normal to the surface. Light incident on the surface of a rugate filter will be reflected in a narrow spectral range, the spectral position of which is dependent on the

[*] Prof. M. Gal, Dr. T. Böcking, S. Ilyas
School of Physics, University of New South Wales
Sydney 2052 (Australia)
E-mail: m.gal@unsw.edu.au
Prof. J. J. Gooding, K. A. Kilian, Dr. T. Böcking
School of Chemistry, University of New South Wales
Sydney 2052 (Australia)
E-mail: justin.gooding@unsw.edu.au
Dr. K. Gaus, Prof. W. Jessup
Centre for Vascular Research, School of Medical Sciences
University of New South Wales
Sydney 2052 (Australia)

[**] We would like to thank the Australian Research Council for funding and Viera Piegerova at the University of New South Wales, Electron Microscopy Unit for assistance with SEM.

ADVANCED FUNCTIONAL MATERIALS

refractive index of the material. Adsorption of material into the rugate filter results in a change of the refractive index which shifts the position of the high reflectivity peak. Correlating the quantity of biological species introduced to the shift in the high reflectivity peak provides the transduction mechanism. Importantly, the high reflectivity peak is easily tunable to the near-IR enabling detection of biological events subcutaneously and intravascularly, providing potential for in vivo photonic devices.[10]

Previously, porous silicon photonic crystals have found utility as in vitro biosensing transducers.[11–16] Surprisingly, little emphasis has been made towards integrating porous silicon photonic materials with medical devices. Towards this goal, we are interested in using porous silicon rugate filters for monitoring molecules in biological fluids and surrounding tissue, with an emphasis on clinical monitoring and diagnosis. In order to enable porous silicon to be used in complex biological environments, the first step after fabrication is chemical functionalization to protect the freshly etched surface from dissolution in aqueous environments. Frequently, porous silicon is oxidized prior to use and subjected to silane chemistry.[12–14] Alternatively, hydrosilylation chemistry has been demonstrated on flat and porous silicon to stabilize the surface[17] with hydrophobic layers providing the most protection from aqueous solutions.[18–21] The potential of hydrophobic surface chemistry for monitoring biological samples is limited by incomplete infiltration of aqueous solutions[22] and surface biofouling from non-specific adsorption of biomolecules.[23] Methods to combat biofouling include antifouling coatings to resist non-specific adsorption and size-exclusion to prevent the ingress of fouling molecules.[24] For the former, covalent modification of surfaces with molecules containing oligo(ethylene oxide) (OEO) moieties has been demonstrated as a robust chemical methodology to reduce biofouling[25] and recently, derivatization of silicon surfaces with OEO molecules has been demonstrated.[26–31] No reports on this antifouling chemistry in porous silicon structures have yet been made.

The purpose of this paper is to present a methodology in modifying porous silicon rugate filters towards in vivo/*ex vivo* optical materials for medical applications. Accurate assessment of biological events will require the following criteria to be met: the material must allow penetration of biological fluid, resist biofouling and maintain stability under physiological conditions for timescales associated with clinical monitoring. We took a combined approach of size-exclusion and antifouling surface chemistry to reduce non-specific adsorption of large globular proteins whilst protecting the underlying substrate from the physiological environment. To simultaneously evaluate the size-exclusion characteristics of the mesopores and the antifouling surface chemistry, we compared rugate filters modified with undecylenic acid monolayers (which have no particular antifouling behaviour) to rugate filters that have been modified with antifouling chemistry. Infiltration of radiolabelled proteins of different size into the two materials provides information on both the antifouling behaviour and the size-exclusion characteristics. Device stability was evaluated by incubation in human blood plasma at physiological temperature and pH. All chemical modification steps, protein infiltration and resistance as well as biological stability were monitored by Fourier transform infra red (FTIR) spectroscopy concurrently with optical characterization of the photonic crystal. Demonstration of feasibility in vitro will pave the way for future developments of porous silicon advanced materials, leading to optical devices for in vivo and *ex vivo* monitoring.

2. Results and Discussion

2.1. Preparation and Characterization of Porous Silicon Rugate Filters

To evaluate the potential of porous silicon (PSi) to operate as a size-exclusion filter, current densities and doping type were chosen for the present study to yield mesopores < 50 nm. Guided by our earlier work,[9,32] mesoporous rugate filters were constructed over a range of parameters towards optimization of the structures for organic derivatization. Rugate filters were selected for this work on account of the low porosity difference between alternating layers. The low porosity difference is important to allow biomolecular diffusion to proceed unimpeded, a potential issue with some multilayered photonic materials where there is a large change in porosity.[14] Assessing the filter quality with regard to optical integrity and chemical stability led to the choice of 40 layer rugate filters that showed high structural stability during chemical modification with a high reflectivity peak. Figure 1 shows the reflectance spectra of a typical batch of rugate filters produced in the electrochemical etching cell, demonstrating the reproducibility achieved. The

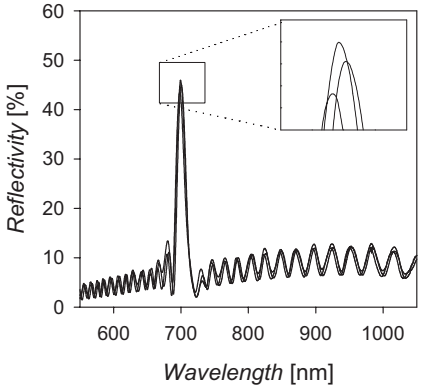

Figure 1. Reflectivity spectrum of freshly etched rugate filters demonstrating the fabrication reproducibility.

full width half maximum (FWHM) of the high reflectivity peak was at (14.7 ± 0.6) nm with very little deviation in peak position (inset, (700 ± 0.4) nm). A scanning electron micrograph of the entire 40 layer structure is shown in Figure 2a. The contrast between layers of alternating porosities is difficult to discern, because of the small variation between high porosity and low porosity layers. This is in contrast to other optical structures such as Bragg mirrors where there is a relatively large porosity

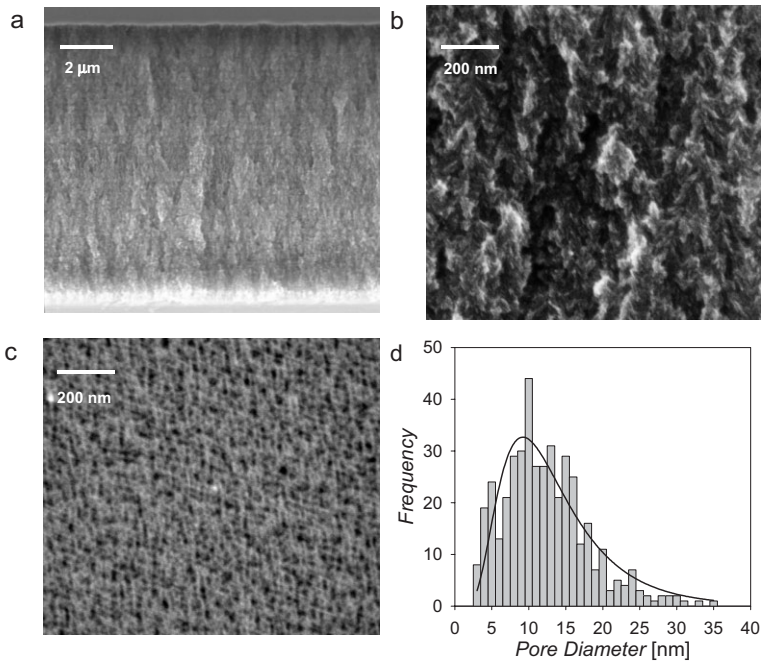

Figure 2. a) Side view scanning electron micrograph of a 40 layer rugate filter, b) close up demonstrating a branched pore morphology, c) top view showing the pore sizes across the surface and d) histogram of the pore size distribution.

differential, yielding abrupt edges. Index matching at the air/PSi and PSi/Si interface to reduce the magnitude of the interference fringes in the spectral background is evidenced by the difference in contrast at the surface and base of the structure. Figure 2b shows a close-up of the structures pore morphology, demonstrating a branched pore network. The pore morphology has a comparable branched appearance to a similar material presented in an earlier report that analysed a range of dopants, doping levels and current densities.[33] From the top view (Fig. 2c), we see a range of pore sizes < 50 nm. Figure 2d shows a histogram of the pores across the surface, 90 % of which are distributed within the 4–20 nm range with an average pore size of 12 nm (± 6 nm). As the majority of the pores are < 20 nm, it is expected that large globular protein are prevented from infiltration whilst small analytes and proteins are able to enter the structure, thus providing some size selectivity.

2.2. Organic Derivatization and Optical Characterization

In order to allow aqueous solutions to infiltrate into the rugate filters while protecting the surface of the porous silicon from oxidation, we chose undecylenic acid as a base layer for hydrosilylation. Undecylenic acid has been shown to produce tightly packed monolayers on porous silicon surfaces and the carboxylic acid functionality renders the surface hydrophilic while providing a convenient functionality for coupling of amines.[34] In Scheme 1, steps a and b depict a pore wall before and after passivation with undecylenic acid. Transmission FTIR of the freshly etched rugate filter shows the ν_{Si-Hx} ($x = 1$, 2, and 3) stretching between 2149 cm^{-1} to 2107 cm^{-1} and ν_{Si-H2} bending modes at 914 cm^{-1} in Figure 3a. After hydrosilylation of undecylenic acid overnight, high monolayer coverage is demonstrated by the reduction in the ν_{Si-Hx} stretching modes and the appearance of peaks characteristic of undecylenic acid monolayers (Fig. 3b). Stretching attributed to symmetric and asymmetric ν_{C-H} modes appear at 2926 cm^{-1} and 2856 cm^{-1} along with a prominent $\nu_{C=O}$ stretch corresponding to the terminal carboxylic acid at 1716 cm^{-1}. A good measure of monolayer quality after hydrosilylation is the level of silicon dioxide formed with less oxide or related species indicating higher efficiency of reaction. Thus the lack of silicon dioxide (1050 cm^{-1}) or back-bonded oxygen $\nu_{O-Si-Hx}$ (2200 cm^{-1}) formed in the reaction are evidence of a high quality monolayer.

After successful passivation of the rugate filters with undecylenic acid monolayers, an anti-fouling layer was next attached to the surface. Covalent attachment of the antifouling layer on the undecylenic acid terminated surface occurred in two steps. Scheme 1b and c illustrates the first step, the activation of the carboxylic acid with *N*-ethyl-*N*′-(dimethylaminopropyl) carbodiimide (EDC) followed by reaction with *N*-hydroxy succinimide (NHS), a common activation technique for amide bond formation. The

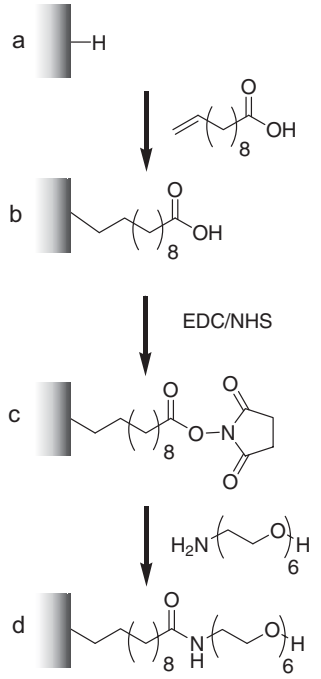

Scheme 1. Derivatization strategy for forming antifouling layers on porous silicon. a) and b) hydrosilylation of 0.2 M undecylenic acid in mesitylene at 120 °C, b) and c) 1-hour activation with 0.1 M EDC and NHS, and c) and d) 4-hour coupling of 20 mM amino EO_6.

EDC activation and coupling to NHS (Fig. 3c), is shown in the FTIR by the appearance of a sharp $\nu_{C=O}$ ester stretch at 1744 cm^{-1} and characteristic succinimide modes at 1791 cm^{-1}

ADVANCED FUNCTIONAL MATERIALS

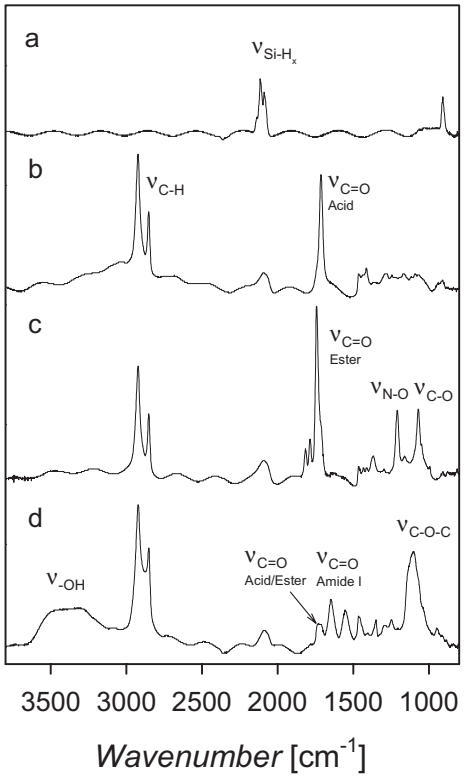

Figure 3. a) FTIR spectra of rugate filters upon organic modification as depicted in Scheme 1. a) Freshly etched surface, b) hydrosilylation of undecylenic acid, c) activation of carboxylic acid with EDC/NHS, and d) coupling of aminoEO$_6$.

the optical properties. The position of the reflectivity maximum in porous silicon rugate filters is dependent on the average refractive index of the PSi.[8,9,32] Replacing air with organic species in the porous layers results in an increase in the refractive index (refractive index $n = 1.0$ for air to $n > 1$ for organic) and a subsequent red shift in the peak position to higher wavelength. Figure 4 shows the shifts in peak position upon chemical modification. The freshly etched rugate filter has a peak position at

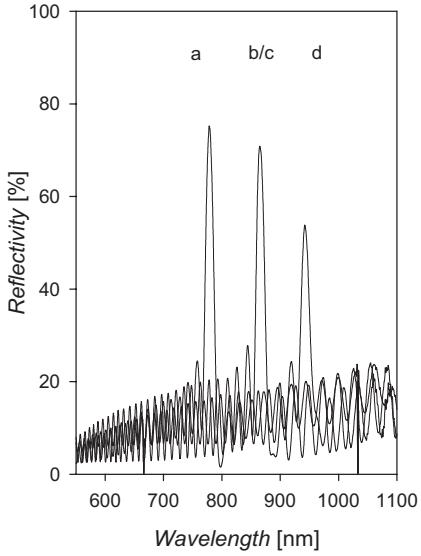

Figure 4. Shift in the high reflectivity peak of reflected light after chemical modification from a–d.

and 1822 cm^{-1}. Further evidence for formation of the NHS ester comes from the stretching of ν_{C-O} at 1075 cm^{-1} and ν_{N-O} at 1214 cm^{-1}. Next in forming the antifouling layer is coupling of the aminoEO$_6$ moiety (Scheme 1c and d). This reaction proceeded under mild conditions over 4 h. Figure 3d clearly shows the disappearance of the NHS ester peaks and the appearance of the amide I ($\nu_{C=O}$) and amide II (ν_{N-H}) modes at 1652 cm^{-1} and 1562 cm^{-1}, respectively. Also of note is the new peak at 1117 cm^{-1} indicative of the ether stretching ν_{C-O} of the ethylene oxide moieties and the broad peak at 3200–3600 cm^{-1} for the ν_{OH} stretch of terminal hydroxyl groups. The small peak at 1715 cm^{-1} verifies some remaining carboxylic acid groups from competing hydrolysis of the NHS ester. Again, there is no evidence of appreciable levels of silicon dioxide (1050 cm^{-1}) or backbonded oxygen $\nu_{O-Si-Hx}$ (2200 cm^{-1}) formed throughout the derivatization procedure, attesting to the quality of the original undecylenic acid base layer in protecting the underlying silicon surface from the ingress of water. (A small quantity of silicon dioxide is presumably present in the structure (~1050 cm^{-1}) but is masked by the dominant ν_{C-O-C} stretching in the FTIR spectrum of the ethylene oxide moieties (1117 cm^{-1}). Significant levels of silicon dioxide would appear as a well-defined shoulder to this peak, which is not readily apparent in the displayed spectrum.)

During the chemical modification, maintaining the structural integrity of the rugate filters was also verified by monitoring 780 nm (a). Monolayer formation of undecylenic acid leads to an 86 nm shift to 865 nm (b). After NHS activation and coupling of aminoEO$_6$, the peak position shifts a further 78 nm to 943 nm (Fig. 4d) inline with expectations of an increase in average refractive index upon incorporation of additional organic material. (These reflectivity shifts are from a single experiment and are representative of typical optical responses observed. The FTIR data is from the same sample used in the reflectivity measurements.) The positive shift after modification is consistent with FTIR data that shows no detectable oxide formation on the PSi. Replacing the bulk silicon of the PSi with silicon dioxide ($n = 3.5$ for silicon to $n = 1.4$ for silicon dioxide) would blue shift the reflectivity maximum to lower wavelength. Importantly, the full width half maximum (FWHM) of the peak remains relatively unchanged during the chemical steps at 14–16 nm. Inhomogeneities or structural instability will lead to broadening of the reflectivity peak. Note that the sharp reflectivity and narrow linewidth is maintained throughout the procedure, a testament to the quality of the chemistry and an important criteria for sensitivity when monitoring small changes at the biological interface. A decrease in the magnitude of the high reflectivity peak occured over the course of organic derivatization, presumably due to decreased homogeneity in the porous layers upon multiple modifications. Nevertheless, the peak remains well above background enabling easy discernment of the optical changes.

2.3. Protein Infiltration and Resistance to Biofouling

Having established stable monolayer formation on the rugate filters, the infiltration characteristics of different sized radiolabelled proteins was assessed. Firstly, infiltration of aqueous media into the structures was verified optically. Rugate filters with undecylenic acid monolayers and EO_6 layers both allowed complete penetration of water as determined by a shift in the high reflectivity peak of ~80 nm as expected for replacing air with water in the pores (data not shown). Three different proteins of size 14 200 Da (α-lactalbumin, approximate size $\sim 2.3 \times 2.6 \times 4$ nm^3), 29 000 Da (carbonic anhydrase, $\sim 4 \times 4 \times 5$ nm^3) and 66 000 Da (bovine serum albumin, $\sim 4 \times 10 \times 14$ nm^3) were chosen to evaluate antifouling properties of the EO_6 layer and the size-selectivity of the porous material. Figure 5a shows the surface mass density of the radiolabelled proteins adsorbed into undecylenic acid and EO_6 modified rugate filters. Carbonic anhydrase adsorption to

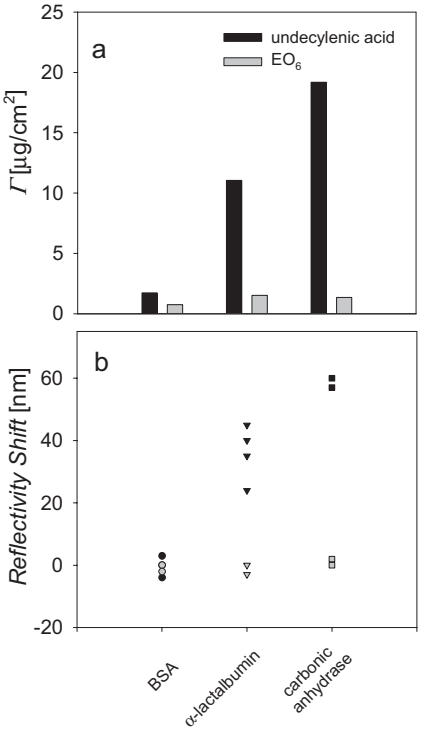

Figure 5. a) Surface mass density of radiolabelled protein adsorbed to the undecylenic acid (black) and EO_6 (grey) rugate filters. b) Reflectivity shift observed corresponding to adsorbed protein.

undecylenic acid surfaces is the highest, leading to an average reflectivity shift of 59 nm in the optics (Fig. 5) while α-lactalbumin produces a smaller shift of 36 nm with BSA resulting in no discernible shift.

Observing the change in the reflectivity maximum with adsorbed radiolabelled protein shows a correlation between mass of adsorbed protein and optical shift expected for an increase in the average refractive index of the structure. The low level of adsorbed protein mass and the negligible change in the optics for bovine serum albumin is attributed to the inability of proteins ≥66 kDa to fully enter the pores of this material. At these pore dimensions, small proteins selectively entered the structure while larger proteins were excluded. This result is not surprising considering 80 % of the pores (including the contribution from the organic layer) are smaller than BSA's longest side and adsorption at the entrance of the largest pores will effectively block additional diffusion into the structure. Although size exclusion prevented the fouling of the rugate filter by BSA it is equally clear the smaller proteins adsorb to the undecylenic acid surfaces, requiring an antifouling surface chemistry.

Initially, to provide a comparison to previous studies, the antifouling behaviour of the EO_6 layer was investigated on flat Si(100) using a procedure by Hamers.[35] Application of FITC-BSA to flat Si(100) surfaces followed by incubation in elution buffer was monitored by fluorometry. Taking the theoretical coverage of a monolayer of BSA on the Si(100) surface to be 0.078 µg cm^{-2} (complete surface monolayer) we see 0.077 µg cm^{-2}, 98 % of a BSA monolayer adsorbed on the flat Si(100) undecylenic acid sample (see Supporting Information, Fig. ES1). In comparison the anti-fouling EO_6 surface showed only 0.008 µg cm^{-2} adsorbed (~10 % BSA monolayer). These results agree closely with those reported for other chemistries incorporating oligo(ethylene oxide) layers on silicon.[35]

The question remains however as to whether this antifouling behaviour on flat surfaces correlates to antifouling behaviour on porous structures. This question is important as antifouling behaviour has never previously been demonstrated on PSi. Comparing the undecylenic acid modified porous silicon surfaces to the EO_6 terminated surface in Figure 5 clearly shows a dramatic reduction of protein adsorbed (60–92 %) confirming the antifouling capabilities of these films. In all cases with EO_6 surfaces there was negligible change in optical peak position and FTIR amide band absorbance, supplementing the results of the fluorescence and radioactivity data. Importantly, no appreciable increase in oxide occurred overnight at room temperature for surfaces with antifouling chemistry suggesting sustained stability.

2.4. Stability in Human Blood Plasma

Earlier reports suggested that the adsorption of proteins to derivatized surfaces result in the structural collapse upon film formation.[23] To evaluate the effect of protein adsorption and resistance in complex media, EO_6 and undecylenic acid surfaces were exposed to blood plasma at 37 °C for up to several days. Work by Canham and co-workers on porous silicon stability demonstrated the structures were highly stable in simulated blood plasma using very hydrophobic monolayers.[10,21] Hydrophobic surface chemistry has been shown to limit infiltration of aqueous solutions and simulated blood plasma neglects effects caused by adsorbed biomolecules.[18,23] Using relatively hydrophilic surface chemistry allows for complete infiltration of plasma into the structure (verified by reflectivity shift from air to aqueous), providing a more realistic environment for assessment of device stability where the fluid must mix with the PSi.

ADVANCED FUNCTIONAL MATERIALS

Figure 6a shows the antifouling EO_6 samples had a negligible change in the reflectivity peak position with no discernable decrease in the reflectivity over a 72-hour period at 37 °C, attesting to the increased stability imparted with antifouling

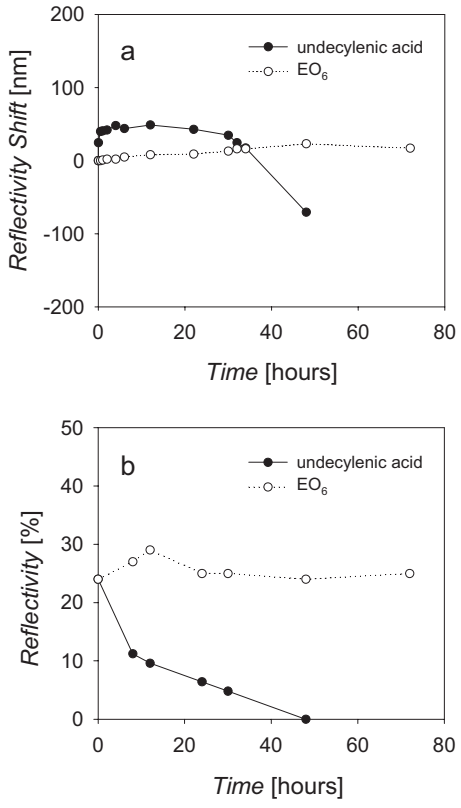

Figure 6. a) Stability of the high reflectivity peak position for undecylenic acid and antifouling EO_6 surfaces exposed to blood plasma over time. b) Stability of reflectivity during blood plasma incubation.

chemistry. In contrast, there was a significant increase in the position of the reflectivity maximum within the first 2 h for the undecylenic acid terminated structure, presumably due to biomolecules <66 kDa in blood plasma adsorbing within the structure (as seen previously with α-lactalbumin and carbonic anhydrase). Shortly after, presumably due to surface oxidation, a steady drift in the peak position is observed along with a degradation of the optics as determined by disappearance of the reflectivity maximum (Fig. 6b).

The marked increase in the stability of the EO_6 surface compared to undecylenic acid in blood plasma at physiological temperature and pH shows the potential for this chemistry to be used in biological applications. Initially, biomolecules from the plasma adsorbed to the undecylenic acid surface causing a red shift in the optics indicating non-specific adsorption. Over time the adsorbed protein aided in dissolution of the porous silicon as evidenced by blue shifting in the spectra and eventual loss of the photonic signature. Structural instability caused by physisorbed protein may account for the dramatic collapse and dissolution of the undecylenic acid surfaces whilst the EO_6 derivatized surfaces maintained their optical integrity for several days. The improved stability and biomolecular resistance of this chemistry over typical timescales of clinical monitoring has the potential for these materials to be integrated as components for in vivo and *ex vivo* medical devices.

3. Conclusion

Adsorbed proteins to the undecylenic acid modified porous silicon rugate filter upon exposure to biological fluid caused accelerated oxidation and eventual structural collapse. Chemical passivation to prevent protein adsorption and oxidation was demonstrated by a multistep derivatization procedure such that the optical integrity was maintained over the period of several days in a complex biological environment. Antifouling chemistry incorporating a hexa(ethylene oxide) moiety was found to be critical in maintaining structural stability and thus, a stable reflectivity in contrast to surfaces with only undecylenic acid monolayers. The ability to have a stable reflectivity profile under physiological conditions will find utility in a number of applications where real-time monitoring of small changes are necessary. For instance, immobilization of biorecognition molecules to the terminal hydroxyl groups of the ethylene oxide units[29] for detecting metabolites or other biological small molecules holds promise for biomarker profiling. Monitoring biological fluids in an *ex vivo* device or as an implant (or component of an implantable device) are both possible. Alternatively, various stimuli, i.e., pH, temperature, light, disease-specific enzymes, could trigger release of immobilised therapeutic compounds, providing a new method of drug delivery. In addition, the flexibility of fabrication and the ability to generate mesoporous particulates[36] enables this material to be used for in vivo labelling of cells and tissue. Molecular size selectivity, increased sample stability and control over spectral reflectivity in the near infra red may allow for remote biophotonic sensing of implantable porous silicon devices, leading to a host of new medical and pharmaceutical research tools as well as advanced diagnostic capabilities for clinical monitoring and point of care devices.

4. Experimental

Chemicals and Reagents: All materials were reagent grade or higher and purchased from Sigma–Aldrich. Si(100) wafers (B-doped 0.07 Ω cm) were purchased from the Institute of Electronics Materials Technology (ITME). Iodine-125 was purchased from Amersham biosciences (IMS30-5MCI) and iodination supplies from Pierce biochemical. Solvents were redistilled prior to use. Mesitylene and undecylenic acid were vacuum distilled and stored over molecular sieves.

Synthesis of Hexa(ethylene glycol) Monophthalimide: Triphenylphosphine (15.5 mmol) was added to a stirred solution of hexa(ethylene glycol) (15 mmol) in dry THF (30 mL). The reaction was cooled on ice and diisopropyl azodicarboxylate (DIAD) (16.5 mmol) was added dropwise over 5 min followed by addition of phthalimide (16.5 mmol). The mixture was brought to room temperature and stirred under an argon atmosphere overnight. The THF was removed under reduced pressure and the crude mixture partitioned between ethyl acetate (50 mL) and water (50 mL). The organic phase was washed twice with water, dried over sodium sulfate and concentrated. The desired product was separated from the crude mixture by column chromatography on silica gel using ethyl acetate to yield a colorless oil in 60 % yield. ^{1}H NMR

(300 MHz, $CDCl_3$): δ 2.85 (s, 1H), 3.54–3.61 (18H), 3.67–3.70 (4H), 3.85 (t, 2H), 7.69 (m, 2H), 7.79 (m, 2H).

Synthesis of Hexa(ethylene glycol) Amine: The phthaloyl group was removed by reaction with 41 % methylamine in water (v/v) at 60 °C for 2 h and phthalic acid partitioned into butanol over 1 M HCl. The aqueous phase was gathered and the crude oil in water subjected to ion exchange chromatography (Analytical Grade Anion Exchange Resin, AG1-X10, BIO-RAD). After removing the water, hexa(ethylene glycol) amine was yielded in 71 %. ^{1}H NMR (300 MHz, $CDCl_3$): δ 2.37 (s, 1H), 2.74 (t, 2H), 3.40 (t, 2H), 3.47 (t, 2H), 3.50–3.57 (16H).

Porous Silicon Rugate Filters: p+-type Si(100), resistivity 0.07 Ω cm, was cleaned in acetone and ethanol with sonication for 5 min each. The wafer was dried and placed in an electrochemical cell as described previously [9]. Briefly, the wafer is back-contacted with a polished steel electrode and the cell filled with 25 % HF in ethanol (equal parts 50 % HF in water and absolute ethanol). A circular platinum electrode is immersed in the ethanolic HF solution above the wafer. A current density alternating between 150 mA cm^{-2} and 250 mA cm^{-2} was applied to the cell sinusoidally with index matching, apodization and current breaks (to retain electrolyte concentration at dissolution front). After etching, the wafer was rinsed with ethanol and pentane, dried with argon and stored until use.

Hydrosilylation, Activation and Coupling: Undecylenic acid and mesitylene (1:2 v/v) were added to a flame dried schlenk flask under argon. The mixture was degassed 4-times under vacuum (freeze/pump/thaw) and the freshly etched porous silicon was added to the flask under positive pressure of argon. The flask was brought to 120 °C and the sample was reacted for 16 h. The sample was rinsed in dichloromethane, ethyl acetate and light petroleum. For activation, undecylenic acid terminated samples were wet with ethanol and incubated in 0.1 M 1-ethyl-3-[3-dimethylaminopropyl]carbodiimide (EDC), 0.1 M *N*-hydroxysuccinimide (NHS) for 1 h at room temperature, rinsed with water, ethanol and dried under argon. Samples were then placed in 20 mM hexa(ethyleneglycol) amine in ethyl acetate or acetonitrile for 4 h at room temperature.

Blood Plasma Experiments: Human blood was collected by venepuncture from healthy subject in accordance with the ethics and safety protocols of the University of New South Wales. Blood was mixed with 2 mM ethylenediaminetetraacetic acid (EDTA), spun at 3000 rpm at 10 °C for 20 min. Plasma was collected, stored at 4 °C and used within 4 days.

Iodination: PD-10 D-Salt™ desalting column (Pierce Biochemical) was equilibrated with 5 washes of 1× PBS. 1 mCi of ^{125}I (100 mCi mL^{-1}, in 0.01 M NaOH solution, pH 8–12.) was added to an iodo-bead™ in an eppendorf tube and incubated for 5 min. 2 mg of lyophilized protein (Sigma, MW-ND-500) was resuspended to 1 mL and added to the iodo-bead with ^{125}I for a 5-minute incubation. The iodinated protein was added to the PD-10 column, eluted with PBS and 1 mL fractions collected. Fractions containing iodinated protein (but not unbound ^{125}I) were determined with a Geiger counter and combined. Protein concentration was determined using a standard BCA reagent assay (Sigma, BCA-1). Eluted protein concentration was between 0.8 and 0.9 μg mL^{-1} and specific activities ranged from 1–10 × 10^4 dpm/ng protein. Ethanol (< 5 % by volume) was applied to the sample to wet the PSi structure and 100 uL of iodinated protein was added to the surface of the porous silicon, keeping the fluid to the porous area to avoid adsorption to the flat silicon edges. The samples were incubated for 4 h in a humid chamber, rinsed twice in PBS, placed in a tube and counted using a COBRA II Auto-gamma counter.

Spectroscopy and Microscopy: Reflectivity spectra were measured by illuminating the sample at normal incidence with a focused monochromatic beam (J/Y SPEX 1681 spectrometer) and detecting the reflected beam using a silicon detector. FTIR spectra were collected using a ThermoNicolet AVATAR 370-FTIR spectrometer with transmission mode and images captured using OMNIC. Scanning electron micrographs were taken using a Hitachi S900 SEM with a 12 kV field emission source.

Received: August 30, 2006
Revised: November 22, 2006
Published online: August 21, 2007

[1] C. K. Mahutte, *Clin. Biochem.* **1998**, *31*, 119.
[2] D. W. Luebbers, *Sens. Actuators B* **1993**, *11*, 253.
[3] K. Tohda, M. Gratzl, *ChemPhysChem* **2003**, *4*, 155.
[4] O. S. Wolfbeis, *Anal. Chem.* **2006**, *78*, 3859.
[5] S. J. Matcher, M. Cope, D. T. Delpy, *Appl. Opt.* **1997**, *36*, 386.
[6] T. M. Battaglia, J.-F. Masson, M. R. Sierks, S. P. Beaudoin, J. Rogers, K. N. Foster, G. A. Holloway, K. S. Booksh, *Anal. Chem.* **2005**, *77*, 7016.
[7] J. Yang, C.-Q. Xu, R. Nutiu, Y. Li, *Proc. SPIE-Int. Soc. Opt. Eng.* **2004**, *5578*, Pt. 1, 109.
[8] W. Theiss, *Surf. Sci. Rep.* **1997**, *29*, 91.
[9] S. Ilyas, T. Böcking, K. Kilian, P. J. Reece, J. J. Gooding, K. Gaus, M. Gal, *Opt. Mater.* **2007**, *29*, 619.
[10] L. T. Canham, M. P. Stewart, J. M. Buriak, C. L. Reeves, M. Anderson, E. K. Squire, P. Allcock, P. A. Snow, *Phys. Status Solidi A* **2000**, *182*, 521.
[11] A. Janshoff, K.-P. S. Dancil, C. Steinem, D. P. Greiner, V. S. Y. Lin, Gurtner, K. Motesharei, M. J. Sailor, M. R. Ghadiri, *J. Am. Chem. Soc.* **1998**, *120*, 12 108.
[12] C. Pacholski, M. Sartor, M. J. Sailor, F. Cunin, G. M. Miskelly, *J. Am. Chem. Soc.* **2005**, *127*, 11 636.
[13] K.-P. S. Dancil, D. P. Greiner, M. J. Sailor, *J. Am. Chem. Soc.* **1999**, *121*, 7925.
[14] H. Ouyang, M. Christophersen, R. Viard, B. L. Miller, P. M. Fauchet, *Adv. Funct. Mater.* **2005**, *15*, 1851.
[15] S. Chan, S. R. Horner, P. M. Fauchet, B. L. Miller, *J. Am. Chem. Soc.* **2001**, *123*, 11 797.
[16] S. Chan, Y. Li, L. J. Rothberg, B. L. Miller, P. M. Fauchet, *Mater. Sci. Eng. C* **2001**, *15*, 277.
[17] J. M. Buriak, *Chem. Rev.* **2002**, *102*, 1271.
[18] R. Boukherroub, S. Morin, D. D. M. Wayner, F. Bensebaa, G. I. Sproule, J. M. Baribeau, D. J. Lockwood, *Chem. Mater.* **2001**, *13*, 2002.
[19] I. N. Lees, H. Lin, C. A. Canaria, C. Gurtner, M. J. Sailor, G. M. Miskelly, *Langmuir* **2003**, *19*, 9812.
[20] J. M. Buriak, M. J. Allen, *J. Am. Chem. Soc.* **1998**, *120*, 1339.
[21] L. T. Canham, C. L. Reeves, J. P. Newey, M. R. Houlton, T. I. Cox, J. M. Buriak, M. P. Stewart, *Adv. Mater.* **1999**, *11*, 1505.
[22] J. T. C. Wojtyk, K. A. Morin, R. Boukherroub, D. D. M. Wayner, *Langmuir* **2002**, *18*, 6081.
[23] L. Tay, N. L. Rowell, D. Poitras, J. W. Fraser, D. J. Lockwood, R. Boukherroub, *Can. J. Chem.* **2004**, *82*, 1545.
[24] N. Wisniewski, M. Reichert, *Colloids Surf. B* **2000**, *18*, 197.
[25] K. L. Prime, G. M. Whitesides, *J. Am. Chem. Soc.* **1993**, *115*, 10 714.
[26] T. Böcking, K. A. Kilian, K. Gaus, J. J. Gooding, *Langmuir* **2006**, *22*, 3494.
[27] C. M. Yam, J. M. Lopez-Romero, J. Gu, C. Cai, *Chem. Commun.* **2004**, 2510.
[28] C. M. Yam, J. Gu, S. Li, C. Cai, *J. Colloid Interface Sci.* **2005**, *285*, 711.
[29] T. Böcking, K. A. Kilian, T. Hanley, S. Ilyas, K. Gaus, M. Gal, J. J. Gooding, *Langmuir* **2005**, *21*, 10 522.
[30] T. Böcking, M. Gal, K. Gaus, J. J. Gooding, *Aust. J. Chem.* **2005**, *58*, 660.
[31] T. L. Lasseter, B. H. Clare, N. L. Abbott, R. J. Hamers, *J. Am. Chem. Soc.* **2004**, *126*, 10 220.
[32] P. J. Reece, M. Gal, H. H. Tan, C. Jagadish, *Appl. Phys. Lett.* **2004**, *85*, 3363.
[33] V. Lehmann, R. Stengl, A. Luigart, *Mater. Sci. Eng. B* **2000**, *69–70*, 11.
[34] R. Boukherroub, J. T. C. Wojtyk, D. D. M. Wayner, D. J. Lockwood, *J. Electrochem. Soc.* **2002**, *149*, H59.
[35] T. L. Clare, B. H. Clare, B. M. Nichols, N. L. Abbott, R. J. Hamers, *Langmuir* **2005**, *21*, 6344.
[36] M. J. Sailor, J. R. Link, *Chem. Commun.* **2005**, 1375.